

ON THE FORMATION OF THE PRIMARY AND SECONDARY VORTEX STREET INSTABILITIES

Elif Bekoglu

Department of Aeronautics
Imperial College London
London SW7 2AZ, UK
e.bekoglu22@imperial.ac.uk

Nikos Bempedelis

School of Engineering and Materials Science
Queen Mary University of London
E1 4NS, London, UK
n.bempedelis@qmul.ac.uk

Konstantinos Steiros

Department of Aeronautics
Imperial College London
London SW7 2AZ, UK
k.steiros@imperial.ac.uk

ABSTRACT

It is widely known that the near wake of bluff bodies is subject to the Karman vortex street instability. It is much less known that a qualitatively similar instability also exists in the far wake, in which large scale vortices form, whether a near-wake von-Karman exists upstream, or not. The cause of this downstream 'secondary' vortex street instability is a source of controversy in the literature. This work presents an experimental (PIV) and numerical (LES) investigation of the wake of solid and porous plates in fully turbulent conditions. The data are analysed using analysis of turbulent statistics and application of modal decomposition techniques. Our results suggest that the secondary street formation is due to the growth and rearrangement of structures that first appear in the very near wake. As the plate porosity is decreased, the secondary vortex formation location is brought upstream, and eventually shares common characteristics with the conventional von-Karman street, possibly suggesting similarities in the formation mechanism of the two types of vortex streets.

Introduction

The instabilities that develop in the turbulent wake have been the subject of widespread research over the last century, as they often give rise to large-scale coherent structures that significantly affect the aerodynamic performance of bluff bodies. The von-Karman vortex street is a notable example: in that case, large scale vortices are generated immediately downstream of the bluff body, inducing periodic loads, and large velocity/pressure fluctuations which significantly alter the mean flow field (Williamson, 1996). Even though vortex shedding has been studied for more than a century, a universal explanation of its emergence has not been put forward. Another example is the so-called secondary vortices (to distinguish them from the primary von-Karman ones) that appear in the far wake of bluff bodies (i.e., tens of diameters downstream (Cimbala *et al.*, 1988)). These vortices are of interest because they have been connected to the phenomenon of wake meandering, which has important consequences in wind farm design (Gupta & Wan, 2019). From a more fundamental perspective, the for-

mation mechanism of secondary vortices is of interest as it is connected to the postulation of Townsend (1976) regarding the onset of self-similarity in turbulent shear flows. In particular, given that these structures appear in flow regions where the mean velocities are self-similar, it is important to distinguish whether their formation is linked to the initial conditions of the flow (i.e., the bluff body) or not. If they do, Townsend's proposition that self-similarity presupposes the loss of memory of initial conditions from the flow comes into question (see Bevilaqua & Lykoudis (1978) and Steiros *et al.* (2024) for a more thorough discussion on the matter).

It is thus important to verify whether the secondary street is a product of the local velocity shear (i.e., if it arises independently of the initial conditions of the flow) or of the small-scale vortices that exist much earlier on, very close to the plate. Both explanations have been put forward in the literature (Cimbala *et al.*, 1988; Huang & Keffer, 1996), and Townsend himself was in favour of the first one (Townsend, 1976). Cimbala *et al.* (1988) performed a local linear stability analysis of the mean flow profile in the wake of various bluff bodies, and recovered the characteristic frequency of the secondary street. From this they inferred that the secondary street is caused by the mean shear, independently of the initial conditions. However, local stability analysis of the mean flow is successful in finding the correct frequencies even in the case of vortex shedding near the body (Triantafyllou *et al.*, 1987), where initial conditions cannot be assumed to be negligible. Huang & Keffer (1996) examined the evolution of the power spectral densities derived from cross wire measurements acquired in the wake of a porous plate. They found that the initial, near-wake spectral peak connected to the shear layer instability, at each of the two shear layers of the wake, gradually increased in magnitude and decreased in frequency as the hot wire moved downstream. From this, Huang & Keffer (1996) postulated that the secondary street appears due to the merging of near wake vortices. However, no direct visual evidence of the above postulated process was provided.

To shed some light on the above, this work presents a joint Particle Image Velocimetry (PIV) and Large Eddy Simulation (LES) study of the near and far regions of the turbulent wake of

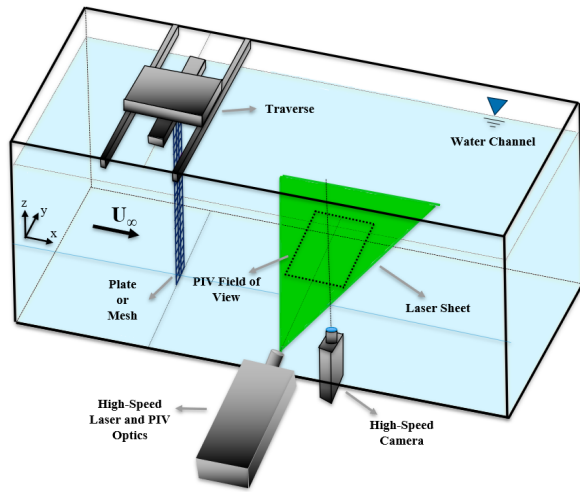


Figure 1. Schematic of the experimental apparatus.

plates and meshes of varying porosity. Our results are in support of the secondary street mechanism postulated by Huang & Keffer (1996), and show a significant influence of the initial conditions on the secondary street dynamics.

The structure of this article is as follows: We first present the details of the laboratory and numerical experiments, and the data processing methods. We then discuss the experimental and numerical results. Finally, we draw the conclusions of this study.

Methodology

PIV measurements

Experiments were conducted in the aeronautics flume of the Aeronautics Department of Imperial College London, which has a square test section of $0.6 \times 0.6 \text{ m}^2$ cross section (see figure 1). The inlet velocity was set to 0.2 ms^{-1} . At that velocity the ambient turbulence intensity was measured to be approximately 1.1%. The primary results concern the testing of a uniform mesh and a porous acrylic plate of 54% and 50% porosity, respectively, that spanned the whole channel. Porosity here is defined as the open area of the mesh/plate over the gross area and was carefully chosen so that the average velocity through the plate/mesh over the free stream velocity, u^* , was identical for the two cases and equal to $u^* = 0.63$. A plate with a porosity of 15% was also tested, so that the effect of the Karman vortex street on the far wake of the bluff body could be documented. The through velocity in that case was measured $u^* = 0.15$. Note that porosities over 20% are known to suppress the vortex street (Castro, 1971). All tested bodies had a width of 3 cm. The Reynolds number based on the plate/mesh width and the free stream velocity was approximately 6,000. High speed PIV was performed at an acquisition frequency of 50 Hz at windows of $35 \times 24 \text{ cm}^2$ size. The PIV windows were positioned at the centreline of flume, and measured a horizontal slice of the flow field. Various downstream locations, ranging from 0 to 80 plate diameters were measured. A 4MP phantom v641 camera was synchronized with a Litron laser using a delay generator. The vector fields were obtained with the DaVis software using multi-pass cross-correlation (final pass of 16 px).

Large Eddy Simulations

Large eddy simulations were carried out using Xcompact3d (Bartholomew *et al.*, 2020), an open-source finite difference framework dedicated to the study of turbulent flows. The simulations employed 6th-order compact schemes and a 3rd-order Adams-Bashforth method. The Reynolds number was $Re = 5000$, with the standard Smagorinsky model used for turbulence modelling. The computational domain spanned $100 \times 20 \times 5$ plate widths and was discretised with a uniform grid consisting of $961 \times 193 \times 48$ points. The porous plate was represented with the actuator disk method and was designed so that the average normalized velocity through it was $u^* = 0.66$. The reasoning behind the LES is that they can generate an idealized numerical experiment, in the sense that the ambient turbulence intensity can be set to effectively zero, and the actuator plate can have a fully homogenous porosity. Preliminary measurements (not shown in this article) showed that both those parameters have an important effect on the characteristics of the secondary vortex street.

Modal decomposition techniques

Both Proper Orthogonal Decomposition (POD) and Spectral proper orthogonal decomposition (SPOD) were used to extract the evolution of coherent structures from the PIV and LES data. Conventional POD is a standard technique and is not discussed further. Regarding SPOD, the algorithm described in Towne *et al.* (2018) is used. SPOD solves the eigenvalue problem of the Fourier transform of the two-point space-time correlation tensor (Towne *et al.*, 2018). In that way, modes that optimally represent the second-order space-time flow statistics and oscillate at specific frequencies (i.e. have time-coherence) can be obtained. For each frequency a set of spatial eigenmodes is produced, ranked according to the magnitude of their eigenvalues. If at a given frequency the first (dominant) eigenvalue exhibits a distinctly larger value compared to the remaining eigenvalues, then this signifies the presence of a coherent structure, at that characteristic frequency. This coherent structure can then be visualized by plotting the eigenmode that corresponds to the eigenvalue.

Results and Discussion

Secondary vortex street at high plate porosity

We begin our analysis with a SPOD reconstruction of the LES data shown in figure 2 (the analysis was performed in the cross-wise velocity component). The dominant eigenmodes at three Strouhal numbers (defined as $St = fD/U_\infty$ where f is the frequency, D the plate width and U_∞ the free stream velocity) are plotted. Those Strouhal numbers corresponded to eigenvalues with large values in the SPOD analysis (see figure 3), i.e., these Strouhal numbers are the footprints of coherent structures. Indeed, the plotted dominant eigenmodes of these Strouhal numbers clearly show the presence of coherent vortices. We note that the LES data include 18 cycles of the secondary vortex street, and cannot therefore be considered perfectly converged (future work will address that). However, the qualitative dynamics depicted are not expected to be drastically altered with increased convergence.

Inspection of the top mode, corresponding to a Strouhal number $St = 0.4$, reveals the existence of small vortices located at the shear layers of the near wake, which are likely the continuation of earlier Kelvin-Helmholtz instabilities. We note that at that plate porosity the primary vortex street is suppressed due to the large fluid bleeding from the plate (Castro, 1971). These vortices seem to disappear at a downstream

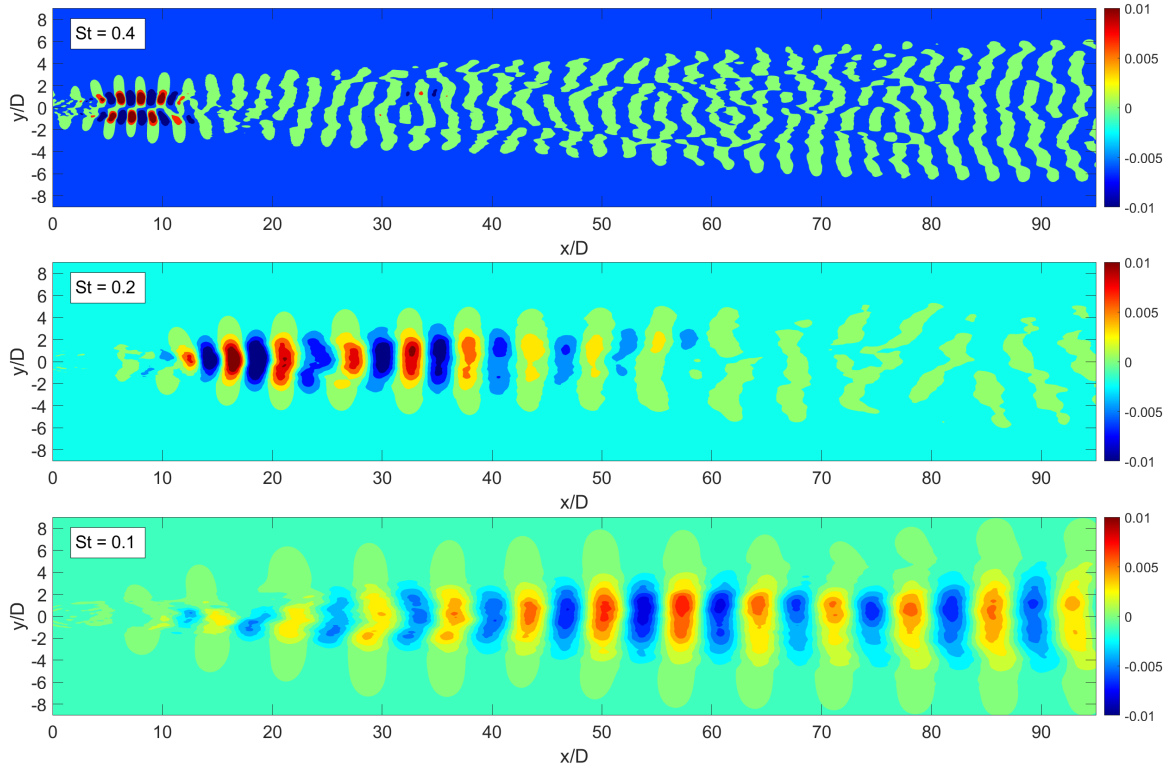


Figure 2. First (dominant) eigenmodes, calculated using SPOD, for the cross-wise velocities at the wake of a $u^* = 0.66$ actuator plate, simulated via LES and situated at $x/D = 0$. The first eigenmodes of three different Strouhal numbers are shown.

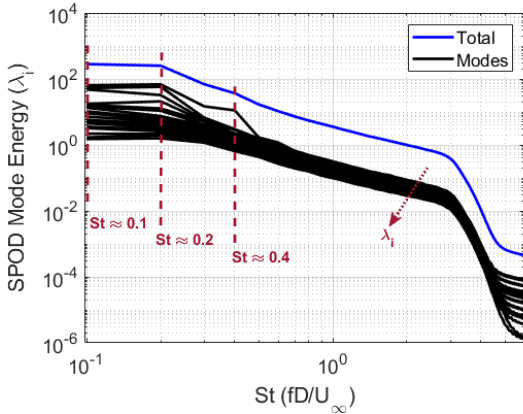


Figure 3. Distribution of SPOD mode energy versus eigenvalue number and Strouhal number.

distance of $x/D \approx 12$, at a location where the middle mode ($St = 0.2$) shows that larger vortices emerge. These vortices span the whole plate width, and are the so-called secondary vortex street (Cimbala *et al.*, 1988; Huang & Keffer, 1996). In turn, these larger structures disappear at a distance of approximately 45 plate widths downstream. At that point, even larger structures emerge (see mode $St = 0.1$), persisting until the end of the numerical domain. The above picture is also indicative of what is observed in the SPOD analysis of the PIV data, but in the case of LES the picture is much clearer, due to the ideal nature of the LES numerical experiments (see section Large Eddy Simulations above).

This flow picture could be thus thought to be in support of the postulation of Huang & Keffer (1996), i.e., that the large secondary street vortices are somehow connected to smaller

vortices close to the plate. In fact, the $St = 0.4$ SPOD mode shows shear layer structures that are reminiscent of the vortices that were reconstructed from the hot wire measurements of Huang & Keffer (1996) using Taylor’s hypothesis. However, the SPOD analysis cannot reveal the dynamics of transition of the small to the larger vortices at roughly $20D$. In particular, do the vortices exhibit this increase in size at $20D$ due to an abrupt merging of the earlier smaller vortices, or due to a gradual diffusion and growth of vortices, or perhaps due to a complete disappearance of the small vortices and then an abrupt reorganization of the shear layers into larger structures, as it has been observed in the far wake of flows where the Karman vortex street is prevalent (Cimbala *et al.*, 1988)?

To answer the above, one would need to inspect the dynamic evolution of coherent structures in the instantaneous vorticity field but that is not straightforward given the multi-scale nature of the flow. For instance, figures 4 and 5 show instantaneous snapshots of vorticity, acquired via PIV, for the $u^* = 0.63$ mesh and plate, where it is obvious that a simple visual extraction of coherent structures is unfeasible. To address that, we performed a POD reconstruction of the instantaneous flow fields using a sufficient number of their higher-order modes so that 50% of the POD energy is retained, i.e., aiming to filter-out the small-scale turbulent motions. Figure 7 shows the reconstructed flow field of the $u^* = 0.63$ mesh. The dynamics of the flow are more evident in the time resolved sequence of the reconstructed fields (available upon request) but are also discernible in the instantaneous snapshots: The near wake vortices grow in their respective shear layers until they reach a critical size, and subsequently ‘invade’ the opposing shear layer generating the secondary vortex street. The situation is qualitatively similar for the porous plate of $u^* = 0.63$ and the actuator plate of $u^* = 0.66$.

Figure 8 plots the distribution of mean streamwise velocities and turbulence intensities (the latter defined as

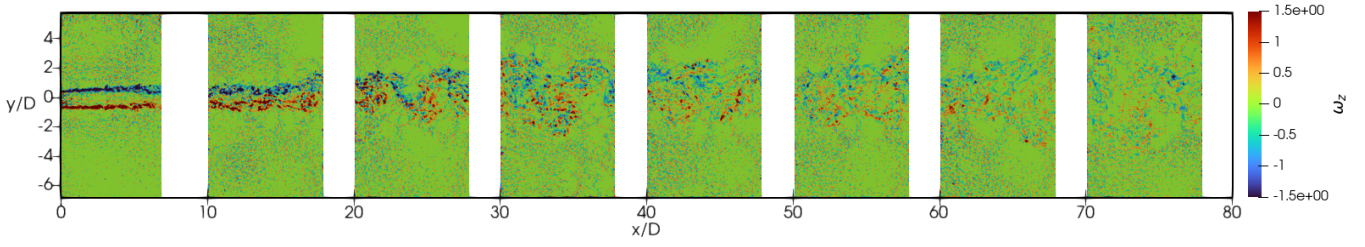


Figure 4. Instantaneous vorticity field, acquired via PIV, for the porous mesh (positioned at $x/D = 0$) of $u^* = 0.63$ and porosity 54%.

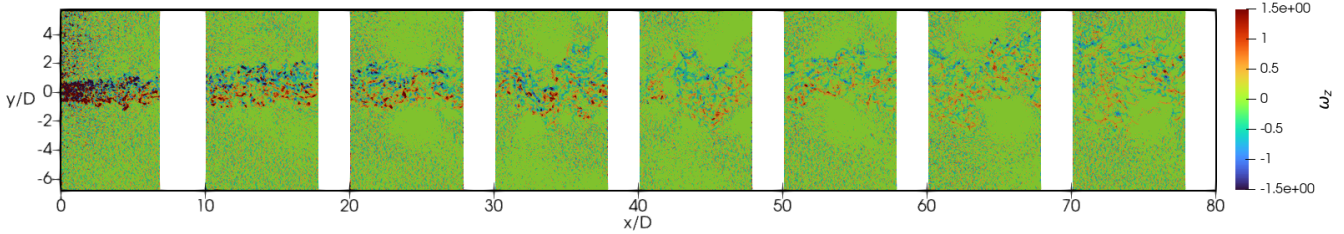


Figure 5. Instantaneous vorticity field, acquired via PIV, for the porous plate (positioned at $x/D = 0$) of $u^* = 0.63$ and porosity 50%.

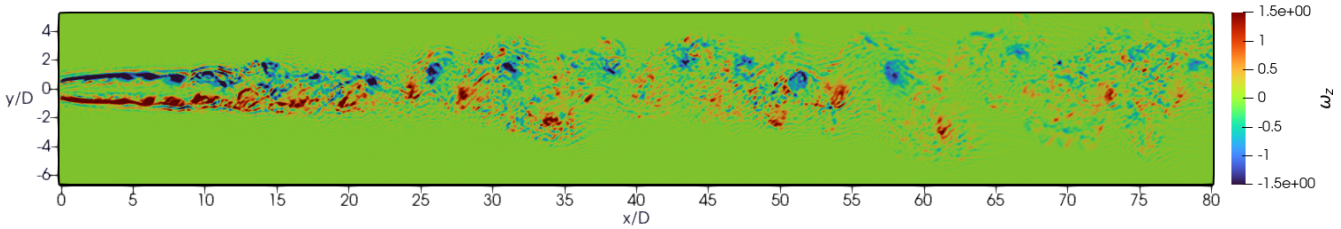


Figure 6. Instantaneous vorticity field, acquired via LES, for the actuator plate (positioned at $x/D = 0$) of $u^* = 0.66$.

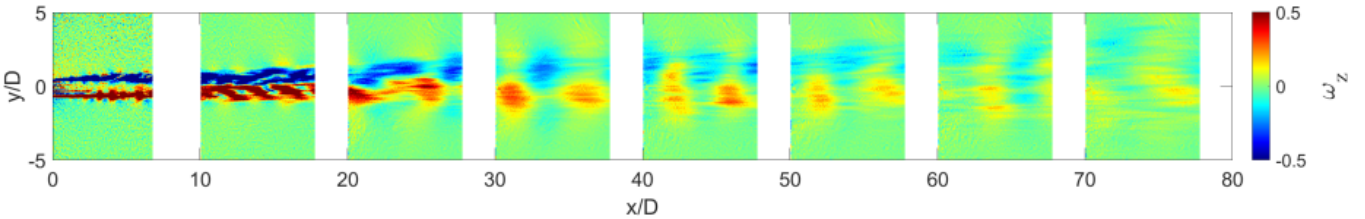


Figure 7. Filtered snapshot of vorticity for the porous mesh of figure 4, by retaining 50% of the POD energy at each measurement plane. In the first two plates (i.e., until $x/D \approx 18$) shear layer vortices are growing, and in the third and fourth planes develop into the secondary street.

$\sqrt{u'^2 + v'^2}/U_\infty$, with u' and v' being the fluctuating components of the streamwise and crosswise velocities, respectively) along the centreline for the $u^* = 0.63$ plate and mesh, as measured by PIV, and the $u^* = 0.66$ actuator plate, simulated via LES. All cases have similar effective porosity (i.e., u^*) and also same momentum deficit in the far wake (i.e., beyond 40 diameters). Still, their flow fields vary considerably, with the relatively near field (up to 20 diameters) exhibiting the most drastic differences: There, the porous plate exhibits very high turbulence intensities in the centreline, and much lower mean streamwise velocities, compared to the mesh and actuator plate cases. This can be attributed to the much larger bulk vorticity values of the porous plate at the near wake which enhance mixing with the outer flow, compared to the mesh and actuator plate cases where vorticity is initially confined in the shear layers and the bulk flow remains unmixed and laminar for longer - vorticity only penetrates the wake beyond 7 diameters downstream (see figures 4 and 6). Given the almost identical effective porosity and far wake momentum deficit (i.e., drag) of the

three bodies, this difference can be attributed to their different inhomogeneity: The pore size of the mesh is roughly ten times smaller compared to that of the porous plate, and will thus generate an order of magnitude smaller vortices, which will decay faster, not being able to sustain turbulent stresses and entrain momentum from the outer wake.

Figure 8 shows that the differences between the three bodies are abated in the far wake (i.e., beyond 30 diameters) but are still persistent. In particular, while the wakes of all three bodies are eventually characterized by almost identical mean centreline streamwise velocities (reflecting an almost identical momentum deficit), there is a clear difference in their turbulence intensities: the wake of the porous plate is characterized by consistently lower values of turbulence intensity compared to the mesh. This is because the mesh, whose near wake is not so well-mixed compared to that of the porous plate, is able to generate a much more coherent secondary street. This can be seen in figure 9, which plots the power spectral densities of the cross-wise velocity component at the centreline location,

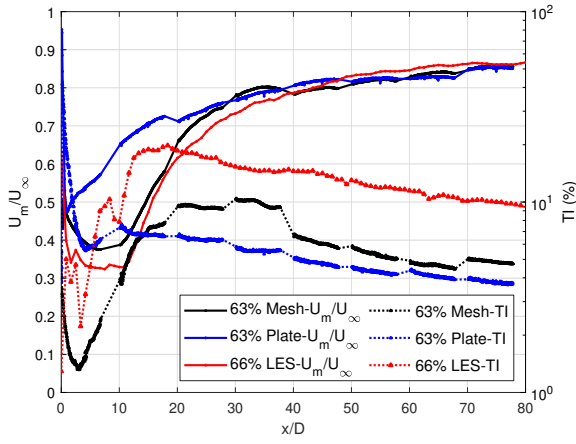


Figure 8. Evolution of mean velocity and turbulence intensity at the centreline, for the plate and mesh of 0.63 normalized through velocity, acquired via PIV, and actuator plate of 0.66 normalized through velocity, simulated via LES.

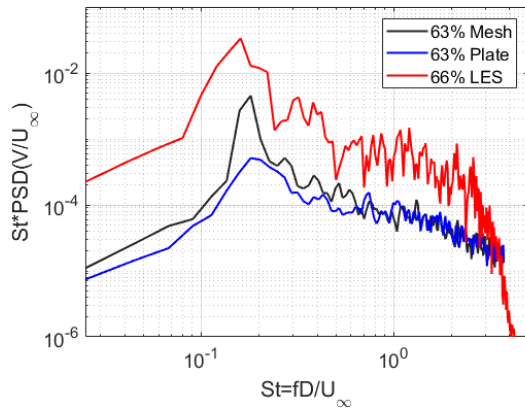


Figure 9. Compensated PSD plots of the normalized cross-wise velocities, for the three highly porous objects, measured at the centreline of the wake, 35 diameters downstream. The peaks at $St \approx 0.18$ are footprints of the secondary vortex street. The percentage in the legend refers to the u^* .

35 diameters downstream of the bodies, and shows a higher spectral peak for the mesh compared to the porous plate. The 'ideal' numerical experiment of the actuator plate (i.e., without ambient turbulence intensity and with a perfectly homogenous plate) produces the largest turbulence intensities (see figure 8), and the highest spectral peak (see figure 9) - it can thus be thought as the limiting, or most favourable case for secondary street formation. The above discussion suggests that, not only that the secondary street is a product of near wake small vortices, but that its evolution is highly dependent on the initial conditions of the flow.

Influence on the primary Karman street

Figure 10 presents a snapshot of the vorticity of the POD reconstructed flow of a porous plate of 15% porosity and $u^* = 0.15$. This configuration is particularly interesting as, contrary to the cases presented above, the plate porosity is not sufficient to completely suppress the Karman vortex street (Castro, 1971). The latter thus appears, but its formation location is transposed from the rear side of the pplate to several

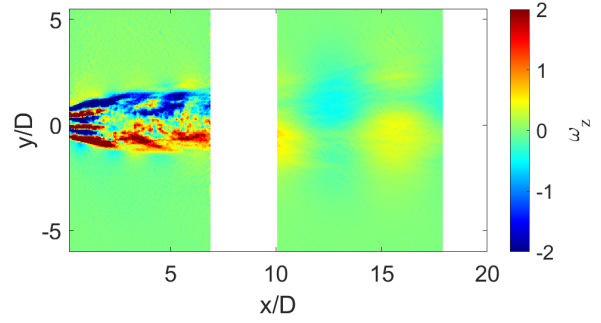


Figure 10. Filtered snapshot of vorticity for the porous plate of 15% porosity, using 60% (first window) and 50% (second window) of the POD energy. A Karman vortex street is observed at the second window ($x/D > 10$).

diameters downstream the plate. The dynamics of the von-Karman street formation are thus exposed in a clearer manner.

The first PIV window in figure 10 ($x/D < 7$) shows a flow picture which is qualitatively similar to the one we described above for the secondary vortex street: Shear layer vortices grow large at their corresponding shear layers, and subsequently seem to move towards the opposing shear layer, forming the von-Karman vortex street in the second PIV window ($x/D > 10$). The above could hint that similar dynamics underpin the formation of the primary and secondary vortex streets.

Conclusions

We have performed a detailed experimental and numerical investigation of the wake of plates and meshes of varying porosity at turbulent Reynolds numbers. The data are analysed via inspection of their turbulent statistics and modal decomposition techniques. Our results suggest that the secondary vortex street forms due to the growth and rearrangement of near-wake vortices, rendering it very sensitive to any change in the boundary/initial conditions. The secondary street structures exist in a flow region which is characterized by self-similarity of the turbulent statistics. Therefore, given that the vortices carry in them information of the initial conditions, this puts in question the assumption that self-similarity presupposes the loss of memory of the initial conditions from the flow. Our results are therefore in agreement with the results of the previous studies of Bevilaqua & Lykoudis (1978) and Steiros *et al.* (2024). Finally, our results hint that the dynamics behind the formation of the secondary vortex street might share common elements.

REFERENCES

- Bartholomew, P, Deskos, G, Frantz, RAS, Schuch, FN, Lamballais, E & Laizet, S 2020 Xcompact3d: An open-source framework for solving turbulence problems on a cartesian mesh. *SoftwareX* **12**, 100550.
- Bevilaqua, PM & Lykoudis, PS 1978 Turbulence memory in self-preserving wakes. *J. Fluid Mech.* **89** (3), 589–606.
- Castro, IP 1971 Wake characteristics of two-dimensional perforated plates normal to an air-stream. *J. Fluid Mech.* **46** (3), 599–609.
- Cimbala, JM, Nagib, HM & Roshko, A 1988 Large structure in the far wakes of two-dimensional bluff bodies. *J. Fluid Mech.* **190**, 265–298.
- Gupta, V & Wan, M 2019 Low-order modelling of wake meandering behind turbines. *J. Fluid Mech.* **877**, 534–560.

- Huang, Z & Keffer, JF 1996 Development of structure within the turbulent wake of a porous body. Part 1. The initial formation region. *J. Fluid Mech.* **329**, 103–115.
- Steiros, K, Obligado, M, Braganca, P, Cuvier, C & Vassiliocos, JC 2024 Turbulent shear flow without vortex shedding, Reynolds shear stress and small scale intermittency. *Under Review*.
- Towne, A, Schmidt, OT & Colonius, T 2018 Spectral proper orthogonal decomposition and its relationship to dynamic mode decomposition and resolvent analysis. *J. Fluid Mech.* **847**, 821–867.
- Townsend, AAR 1976 *The structure of turbulent shear flow*. Cambridge University Press.
- Triantafyllou, GS, Kupfer, K & Bers, A 1987 Absolute instabilities and self-sustained oscillations in the wake of circular cylinders. *Phys. Rev. Lett.* **59** (17), 1914.
- Williamson, CHK 1996 Vortex dynamics in the cylinder wake. *Annu. Rev. Fluid Mech.* **28** (1), 477–539.